International Atomic Energy Agency

INDC(CCP)-365
Distr.: L

INDC INTERNATIONAL NUCLEAR DATA COMMITTEE

MEASUREMENTS OF NEUTRON NUCLEAR DATA OF ACTINIDES

(Translation of selected Russian papers published in Yadernye Konstanty 1987-1991)

Translation editor: Dr. A. Lorenz

February 1994

IAEA NUCLEAR DATA SECTION, WAGRAMERSTRASSE 5, A-1400 VIENNA

Reproduced by the IAEA in Austria
February 1994

INDC(CCP)-365
Distr.: L

MEASUREMENTS OF NEUTRON NUCLEAR DATA OF ACTINIDES

(Translation of selected Russian papers published in Yadernye Konstanty 1987-1991)

Contents

Translation editor: Dr. A. Lorenz

February 1994

MEASUREMENT AND ANALYSIS OF THE RESONANCE STRUCTURE OF THE ^{238}U TOTAL AND RADIATIVE CAPTURE CROSS-SECTIONS IN THE 0.465-200 keV ENERGY RANGE

Yu.V. Grigor'ev, V.N. Koshcheev, G.N. Manturov, V.V. Sinitsa
Power Physics Institute, Obninsk

Yu.S. Zamyatnin
Joint Nuclear Research Institute, Dubna

G.V. Muradyan
I.V. Kurchatov Institute of Atomic Energy, Moscow

N.V. Yaneva, G.P. Georgiev, B.I. Ivanov, I.A. Sirakov
Nuclear Research and Power Institute, Sofia, Bulgaria

ABSTRACT

The total transmission and self-indication functions of the radiative capture cross-section of ^{238}U were measured on the IBR pulsed neutron source by the time-of-flight method. Group-averaged total cross-sections, resonance self-shielding factors and average resonance parameters were obtained and compared with other data.

INTRODUCTION

The only direct information we have about the resonance structure of neutron cross-sections in the unresolved resonance region comes from the measured averaged cross-sections and the total and partial transmission functions. These important integral cross-section characteristics can be used to obtain more precise information on the averaged resonance parameters (strength functions and scattering radii), and to determine the resonance self-shielding factors for cross-sections in the ABBN group

constant system [1, 2] which is used in applied reactor calculations and radiation protection calculations. However, to measure transmission levels we need high-intensity sources and high-efficiency detectors, as well as massive, thick filter samples. For these reasons, experiments of this kind have not been widely performed. To date, we only have adequate measurements for the total transmission levels in uranium-238 samples (over 10 articles). The data given in Refs [3, 4] on the temperature dependence of transmission levels should also be noted. The partial transmission levels for the radiative capture and scattering cross-sections (these are also referred to as self-indication functions) have also been measured and results for them are given in Refs [4-9]. However, these transmission data were obtained mainly using thin filter samples and for a small range of thicknesses. Unfortunately, the discrepancies between the results from these various articles are beyond the limits of experimental error and are not susceptible of a unique interpretation. Since uranium-238 is a highly important raw material in reactors, we need to refine the nuclear data for this isotope using a more advanced experimental technique. To that end, the total transmission levels and self-indication functions for radiative capture in uranium-238 were measured using the 1000 meter time-of-flight beam of the IBR-30, an all-energy neutron detector with ^{3}He counters [5], and a gamma-ray scintillation detector employing NaI(Tl) crystal [10], operating in a multiple coincidence mode . The experimental transmission levels were used to obtain the resonance self-shielding factors and the average resonance parameters in the unresolved energy region.

EXPERIMENTAL METHODOLOGY

The measurements were carried out with the IBR-30 operating in pulsed mode, with a multiplication factor of 200, at an average thermal power of 10 kW and with a neutron pulse duration of 4 μs at half maximum and a burst frequency of 100 Hz. The

total and partial transmission levels were measured simultaneously under good geometry conditions for the 0.1-200 keV energy range. The neutron detector consisting of ring-shaped array of 16 ^{3}He counters (type SNM-18) was positioned 1006 m from the neutron source; a scintillation detector with 16 NaI(Tl) crystals was positioned at a distance of 502 m. The filter samples which comprised disks of metallic ^{238}U 195 mm in diameter, and of different thicknesses were placed in the neutron beam at a distance of 242 m from the neutron source. Both detectors (for neutrons and gamma rays) had apertures to affix radiator samples, spanned a solid angle of almost 4 π steradian and had a radiation detection efficiency of 6% and 80% respectively at the optimum signal detection thresholds. A polyethylene disk 80 mm in diameter and 10 mm thick was used as the radiator sample to measure the total transmission levels, and thin samples of metallic ^{238}U (0.00238 nuclei/b thick and 80 mm in diameter) were placed in the gamma-ray detector to measure partial capture transmission levels, or a background scatterer equivalent sample made of natural lead (0.00316 nuclei/b thick and 80 mm in diameter). In order to reduce the background, boron carbide and cadmium carbide filters were placed permanently in the neutron beam to eliminate multiple neutron scattering. In addition to the external shielding, the gamma-ray detector also had internal shielding in the form of a paraffin and boron carbide absorber with an overall thickness of 65 mm; an evacuated tube was placed through the aperture. Two monitor counters positioned 60 m from the source were used to monitor the source strength. The counter assembly [11] registered all of the signals from the detectors and monitors in the form of time spectra (one from the neutron detector and 16 for the detection of multiple counts from the gamma-ray detector). The counting assembly also processed the spectra and obtained the transmission levels while performing the measurements.

MEASUREMENT RESULTS

During the measurements, time spectra were recorded over the 110 eV to 10 MeV energy range with seven different filter thicknesses positioned in and out of the neutron beam. These spectra were compressed into a smaller number of channels to fit the boundaries of the energy groups of the ABBN group structure. The transmission levels were expressed in terms of integral characteristics of the cross-sections:

$$T_x(n)=\frac{N(n)-\{F_v(n)+F_c(n)\}}{N(O)-\{F_v(O)+F_c(O)\}}\cdot\frac{M(O)}{M(n)}=\int_{\Delta E}\varphi(E)\epsilon(E)e^{-\sigma_t(E)n}dE\Big/\int_{\Delta E}\varphi(E)\epsilon(E)dE, \quad (1)$$

where $T_x(n)$ is the total transmission level or self-indication function for a sample of thickness n; $\varphi(E)$ is the neutron beam spectrum; $\epsilon(E)$ is the detector efficiency; $\sigma_t(E)$ is the total cross-section; N(n), N(O) are the number of detector counts with the filter sample in and out of the beam respectively; $F_v(n)$, $F_v(O)$ are the variables defining the background; $F_c(n)$, $F_c(O)$ are the constants defining the background; and M(n), M(O) are the number of monitor counts.

Equation (1) can be used to determine the total transmission levels and the self-indication functions. In the latter case, the detector efficiency is proportional to the radiative capture cross-section, which also predetermines the self-shielding amplification effect in the resonance cross-section. The constant background level in the spectra was determined from the low tungsten and cadmium resonances (samples of tungsten and cadmium were placed permanently in the neutron beam).

When measuring spectra with the gamma-ray detector for a specific filter sample thickness, the variable components of the background were determined using the lead scatterer equivalent from the following equation:

$$F_v = N(Pb)\frac{n(U)}{n(Pb)}\cdot\frac{\sigma_s(U)}{\sigma_s(Pb)}\cdot\frac{T_s(U)}{T_t(U)}\cdot\frac{M(U)}{M(Pb)} \qquad (2)$$

where N(Pb) is the number of neutrons scattered by the lead sample; n(U) and N(Pb) are the number of nuclei per cm^2 for a uranium and lead radiator sample; $\sigma_s(U)$ and $\sigma_s(Pb)$ are the mean scattering cross-sections for uranium and lead respectively; $T_s(U)$ is the partial transmission value of the uranium scattering cross-section; $T_t(U)$ is the total uranium transmission level; and M(U) and M(Pb) are the number of monitor counts in the measurements with a uranium and lead radiator sample. The variable background was also determined using resonance filters made of aluminum (35, 85 and 140 keV) and manganese (0.337, 2.4 keV) in the total and partial transmission measurements.

Since the gamma-ray detector measured the time spectra for all coincidence levels, from the first through to the sixteenth, simultaneously, partial transmission levels were obtained for all coincidence levels as well as for the integral channel. It should be noted that the background components in the spectra decrease as the coincidence counts increase. For instance, in the case of spectra from triple coincidences, the background level contribution is 10-100% lower than for the summed spectra. The contributing background components increase as the energy decreases and as the thickness of the filter sample increases from 10% to 95%; the accuracy level for determination of the background levels is approximately 3% and 0.5% respectively. The background level in the neutron spectrum was no more than 15% over a wide energy range and depended only slightly on the thickness of the filter.

The resulting experimental transmission values are shown in Table 1. The uncertainty for these values range from 1-2% for lower attenuation levels and increase to 10-30% for transmission values of 0.1-0.05. Fig.1 shows that the self-indication functions for various coincidence levels fall within the error limits.

ANALYSIS OF MEASUREMENT RESULTS

At high energies, the total and partial transmission levels coincide within the limits of experimental error, which indicates that there are no resonance self-shielding effects in the radiative capture cross-section. The non-exponential shape of the total transmission levels indicates that there is resonance blocking of the total cross-section in all the energy groups shown. The high level of agreement between the total transmission values obtained by us and those given in Ref. [14] should be noted. In Ref. [14], the same 1000 m time-of-flight of the IBR-30 was used to perform the measurements but a different detector was used and the energy resolution was not as good (the neutron burst duration was 100 μs). This can be seen clearly in Figs 2-4 which show the dependence of the observed cross-sections $\sigma_{0bs} = -(1/n)\ln T$ for various sample thicknesses as a function of the neutron energy. Where the sample thicknesses are large the observed total cross-sections approach a constant value which is close to the potential scattering cross-section.

By extrapolating the cross-sections given for small sample thicknesses, we can determine the average cross-sections for zero thickness sample. However, this procedure yields results which are ambiguous owing to the high experimental error levels at $T \approx 1$ and therefore a more acceptable approach is the method of subgroup representation of the average cross-sections, transmission functions and resonance self-shielding factors [12]. In this case, the experimental transmission values are approximated as the sum of exponential functions. Two exponents are sufficient to describe the transmission values in this experiment:

$$T_t(n)=a_1 e^{-\sigma_{t1}n}+(1-a_1)e^{-\sigma_{t2}n};\ \langle\sigma_t\rangle=a_1\sigma_{t1}+(1-a_1)\sigma_{t2}\ , \tag{3}$$

$$T_\gamma(n)=a_{\gamma1} e^{-\sigma_{t\gamma1}n}+(1-a_{\gamma1})e^{-\sigma_{t\gamma2}n};\ \langle\sigma_{t\gamma}\rangle=a_{\gamma1}\sigma_{t\gamma1}+(1-a_{\gamma1})\sigma_{t\gamma2}, \tag{4}$$

$$f(\sigma_o)=\frac{1}{\langle\sigma_t\rangle}\left[\frac{a_1/(\sigma_{t1}+\sigma_o)+(1-a_1)/(\sigma_{t2}+\sigma_o)}{a_1/(\sigma_{t1}+\sigma_o)^2+(1-a_1)/(\sigma_{t2}+\sigma_o)^2}-\sigma_o\right] \quad (5)$$

$$f_\gamma(\sigma_o)=\frac{a_{\gamma1}/(\sigma_{t\gamma1}+\sigma_o)+(1-a_{\gamma1})/(\sigma_{t\gamma2}+\sigma_o)}{a_1/(\sigma_{t1}+\sigma_o)+(1-a_1)/(\sigma_{t2}+\sigma_o)}, \quad (6)$$

where a_1, $a_{\gamma1}$ are the contributions of the first subgroup cross-sections; σ_{t1}, σ_{t2}, $\sigma_{t\gamma1}$, $\sigma_{t\gamma2}$ are the subgroup cross-sections; σ_o is the dilution cross-section; $f_t(\sigma_o)$, $f_\gamma(\sigma_o)$ are the resonance self-shielding factors of the total cross-section and the radiated capture cross-section.

The method of least squares was used to find the optimum subgroup parameters . Table 2 lists the average group cross-sections obtained in our experiment and those of other sources.

The experimental total cross-sections from all the sources used in our comparison [9, 13, 14] agree within the limits of error both with our data and with the evaluated data in Ref. [2]. However, there is a marked tendency towards higher cross-section values in our work and in Ref. [14] where the measurements were also performed on the 1000 m time-of-flight of the IBR-30. It should also be noted that the experimental data reported in Ref. [13] were obtained from the total transmission levels measured using monoenergetic neutrons with an energy resolution of approximately 60% at 10 keV and 10% at 200 keV for a set of filter sample thicknesses ranging from 3 to 50 mm, and their measurement aperture was several times worse than ours. The above-mentioned characteristics of the experiments reported in Refs [9] and [13] could lead to overestimation of the transmission values and, consequently, underestimation of the average group cross-sections.

Apart from the total cross-sections, the resonance self-shielding factors of the ^{238}U neutron cross-sections were

also determined from the subgroup parameters obtained from the transmission levels. The results of this analysis and data from other sources are given in Table 3. The data produced by various authors using the same transmission levels but different techniques, are worth looking at. Thus, the results given in Refs [14] and [15] differ by 30% in some energy groups even though the same source material is being used. Clearly, these discrepancies are caused by the fact that in Ref.[14] the self-shielding factors were determined using the subgroup method whereas in Ref. [15] they were determined using the mean resonance parameters. Ref.[15] also reports lower mean group total cross-section values than Ref. [14].

As can be seen from Table 3, the experimental resonance self-shielding factors which we report agree with the experimental data from Ref. [9] within the limits of experimental error and also do not contradict the results in Ref.[2].

The measurements of the total and capture transmission functions in the 4.65-200 keV energy region were used to evaluate the mean resonance parameters - scattering radii as well as neutron and radiation strength functions. The EVPAR [16, 19] program was used to perform this evaluation.

The EVPAR program allows one to take account of highly heterogeneous experimental information in the evaluation: average, total and partial cross-sections (σ_t, σ_γ, σ_s). Its latest modification also allows one to take account of the transmission functions including those measured using the self-indication technique. The EVPAR program uses the Hauser-Feshbach-Moldauer formalism to calculate the mean cross-sections. The total and partial transmission functions are calculated in a multilevel approximation which takes account of inter-resonance interference, Doppler broadening of resonances and fluctuations in neutron widths. The parameters of the calculation models used in the EVPAR program are the scattering radii R_l, the neutron strength functions S_{nl} and the radiative strength functions $S_{\gamma l}$

for neutron waves with orbital momenta of l = 0,1,2. The program uses the maximum likelihood method to fit the calculated data to the experimental data. It should be noted that the results produced by the EVPAR program can be presented in the ENDF/B format in the form of a section of the corresponding file with energy dependent parameters (MF = 2, MT = 151, LRU = 2, cf. description of formats in Ref.[17]).

Table 4 lists the average resonance parameters obtained by us when describing transmission data and compares them with the results from other sources. The values obtained for the strength functions S_{no} and S_{n1}, and also $\Gamma_{\gamma o}$ and D_o show a high level of agreement with the results obtained by averaging the resolved resonance parameters. With respect to the scattering radii R_l, in order to make the data agree at low and high energies, an energy dependence had to be introduced for the R_l', $R_l = R_l'$ (1-0.2xE MeV)parameters. Figs. 1-4 show the calculated results which we produced for the evaluated parameters along side the experimental results. Fig. 5 also gives the calculated energy dependencies of the ^{238}U total and radiative capture cross-sections and compares them with the experimental data. Table 3 gives the self-shielding factors calculated using the GRUKON program [18] and the evaluated mean resonance parameter values. They are close to the results given in Ref. [15].

In conclusion, it should be noted that the mean resonance parameters, cross-sections and resonance shelf-shielding factors produced from the transmission values agree with the evaluations given in other sources and can therefore be used to produce more accurate neutron constants for ^{238}U.

Table 1

Total and partial transmissions for ^{238}U

№ Gr.	E_{cr} (keV)	n (мм)	1	2	4	8	16	32	64
		n (at/b)	0,00478	0,00958	0,0190	0,0380	0,0764	0,153	0,306
8	200- 100	T_t [14]	–	–	–	–	–	–	–
		T_t	0,961	0,887	0,812	0,668	0,456	0,209	0,045
		T_γ	0,959	0,901	0,830	0,666	0,446	0,219	0,050
9	100- 46,5	T_t [14]	0,935	0,874	0,800	0,629	0,407	0,174	0,038
		T_t	0,939	0,836	0,757	0,644	0,395	0,162	0,0358
		T_γ	0,941	0,901	0,804	0,635	0,424	0,186	0,036
10	46,5-21,5	T_t [14]	0,926	0,866	0,795	0,606	0,373	0,172	0,033
		T_t	0,947	0,861	0,771	0,613	0,387	0,158	0,0358
		T_γ	0,916	0,866	0,764	0,589	0,374	0,142	0,030
11	21,5-10	T_t [14]	0,919	0,883	0,786	0,593	0,376	0,162	0,032
		T_t	0,930	0,856	0,758	0,596	0,376	0,156	0,0365
		T_γ	0,908	0,847	0,744	0,536	0,331	0,123	0,022
12	10 - 4,65	T_t [14]	0,914	0,855	0,766	0,584	0,362	0,167	0,034
		T_t	0,933	0,850	0,751	0,602	0,371	0,157	0,0378
		T_γ	0,922	0,831	0,714	0,519	0,311	0,108	0,023
13	4,65-2,15	T_t [14]	0,914	0,831	0,770	0,560	0,360	0,162	0,045
		T_t	0,908	0,820	0,725	0,581	0,356	0,147	0,0413
		T_γ	0,772	0,724	0,556	0,379	0,377	0,050	–
14	2,15- 1,0	T_t [14]	0,898	0,807	0,759	0,591	0,390	0,186	0,054
		T_t	0,897	0,810	0,718	0,584	0,392	0,186	0,0618
		T_γ	0,636	0,490	0,371	0,248	0,160	0,040	–
15	1,0-0,465	T_t [14]	–	–	–	–	–	–	–
		T_t	0,930	0,844	0,755	0,592	0,436	0,212	0,0646
		T_γ	0,530	0,359	0,304	0,193	0,091	0,039	–

Table 2

Average group cross-sections $\langle\sigma_t\rangle$, $\langle\sigma_{t\gamma}\rangle$ for ^{238}U

Gr.	E_{gr}(keV)	Exp. $\langle\sigma_t\rangle$	Exp. $\langle\sigma_{t\gamma}\rangle$	$\langle\sigma_t\rangle$[13]	$\langle\sigma_t\rangle$[9]	$\langle\sigma_t\rangle$[14]	$\langle\sigma_t\rangle$[2]
8	200-100	11,5±0,3	10,8±0,3	11,7±0,1	-	12,0±0,5	11,53
9	100-46,5	12,8±0,3	12,0±0,3	12,7±0,1	12,4±0,3	13,0±0,5	12,57
10	46,5-21,5	13,9±0,4	14,2±0,4	13,5±0,2	13,7±0,3	14,6±0,5	13,46
11	21,5-10,0	15,5±0,5	17,5±0,8	14,5±0,2	14,6±0,4	16,5±0,5	14,48
12	10,0-4,65	15,5±0,5	20,1±1,0	16,4±0,3	16,5±0,5	17,3±0,8	15,88
13	4,65-2,15	20,7±0,7	111±11	-	-	20,0±0,8	18,95
14	2,15-1,00	24,0±1,0	112±12	-	-	22,2±1,0	22,19
15	1,0-0,465	24,0±1,0	176±18	-	-	24,0±1,0	23,70

Table 3

Resonance self-shielding factors for the total and radiative capture cross-sections for $_{238}U$

Gr	E_{gr}(keV)		Exp.	Calc	[13]	[9]	[14]	[15]	[2]
8	200 - 100	f_t	0,88±0,04	0,957	0,94	-	-		0,950
		f_γ	1,00	0,986	-	-	-	-	0,986
9	100 -46,5	f_t	0,79±0,04	0,926	0,91	0,946±0,029	0,86±0,04	-	0,915
		f_γ	0,96±0,02	0,962	-	0,980±0,014	-	-	0,958
10	46,5-21,5	f_t	0,77±0,04	0,840	0,83	0,864±0,031	0,82±0,05	0,774	0,855
		f_γ	0,94±0,02	0,914	-	0,931±0,024	-	0,879	0,910
11	21,5-10,0	f_t	0,68±0,04	0,657	0,76	0,777±0,035	0,70±0,05	0,544	0,755
		f_γ	0,84±0,03	0,765	-	0,868±0,035	-	0,781	0,830
12	10,0-4,65	f_t	0,68±0,04	0,588	0,68	0,617±0,044	0,60±0,07	0,472	0,668
		f_γ	0,78±0,04	0,666	-	-	-	0,659	0,719
13	4,65-2,15	f_t	0,51±0,03	-	-	-	0,44±0,10	-	0,447
		f_γ	0,51±0,03	-	-	-	-	-	0,501
14	2,15-1,00	f_t	0,36±0,03	-	-	-	0,39±0,10	-	0,407
		f_γ	0,36±0,02	-	-	-	-	-	0,304
15	1,0-0,465	f_t	0,35±0,03	-	-	-	-	-	0,365
		f_γ	0,24±0,02	-	-	-	-	-	0,183

Table 4

Average $_{238}$U resonance parameters

Ref.	$S_{n1} \cdot 10^4$		Γ_γ	D_l (eV)		R_l' Fm	
	l=0	l=1	l=0	l=0	l=1	l=0	l=1
н.р.	1,10+0,05	1,70±0,20	23,5±0,7	20,8*	6,9	9,35	8,0
[3]	0,89+0,01	1,87±0,03	24,8*	20,8*	6,9	9,01	9,01
[19]	0,93+0,03	2,30±0,07	22,9±0,7	20,8*	4,4	9,35	6,70
[20]	1,14	2,0	22,2	21,6	7,2	8,13	9,13
[7]	1,11+0,11	2,20±0,20	22,9±0,9	20,8*	6,9	-	-

* The parameter was fixed at the time of optimization

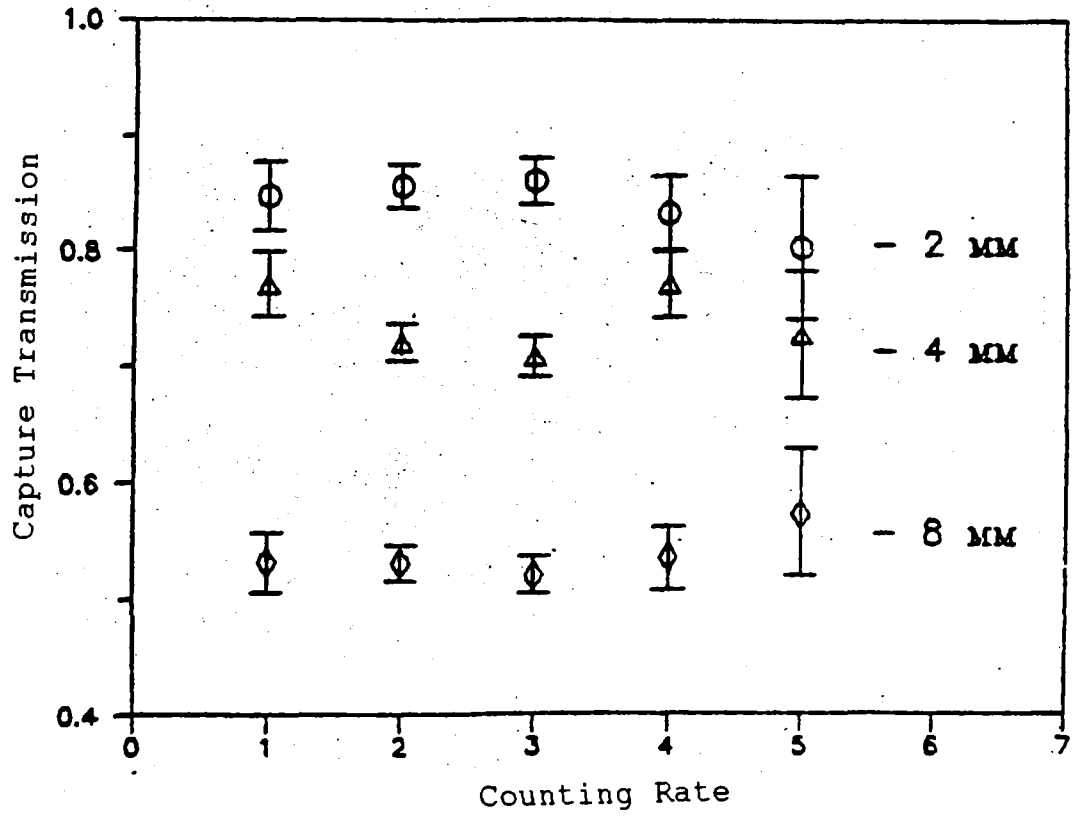

Fig. 1 Dependence of the capture transmission of uranium-238 on the gamma-ray counting rate for different sample thicknesses

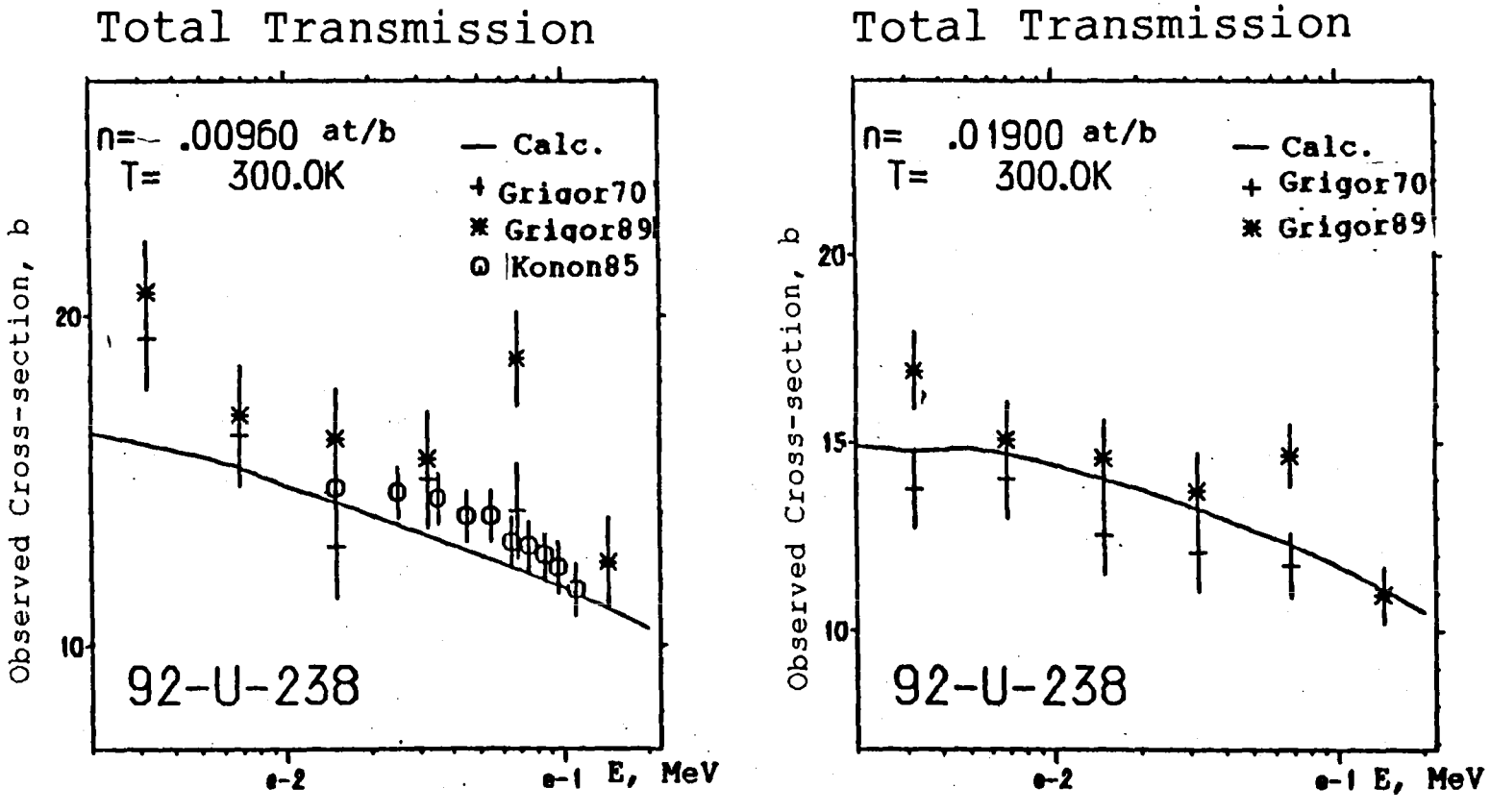

Fig. 2 Energy dependence of the observed cross-section for 2 and 4mm uranium-238 filter samples

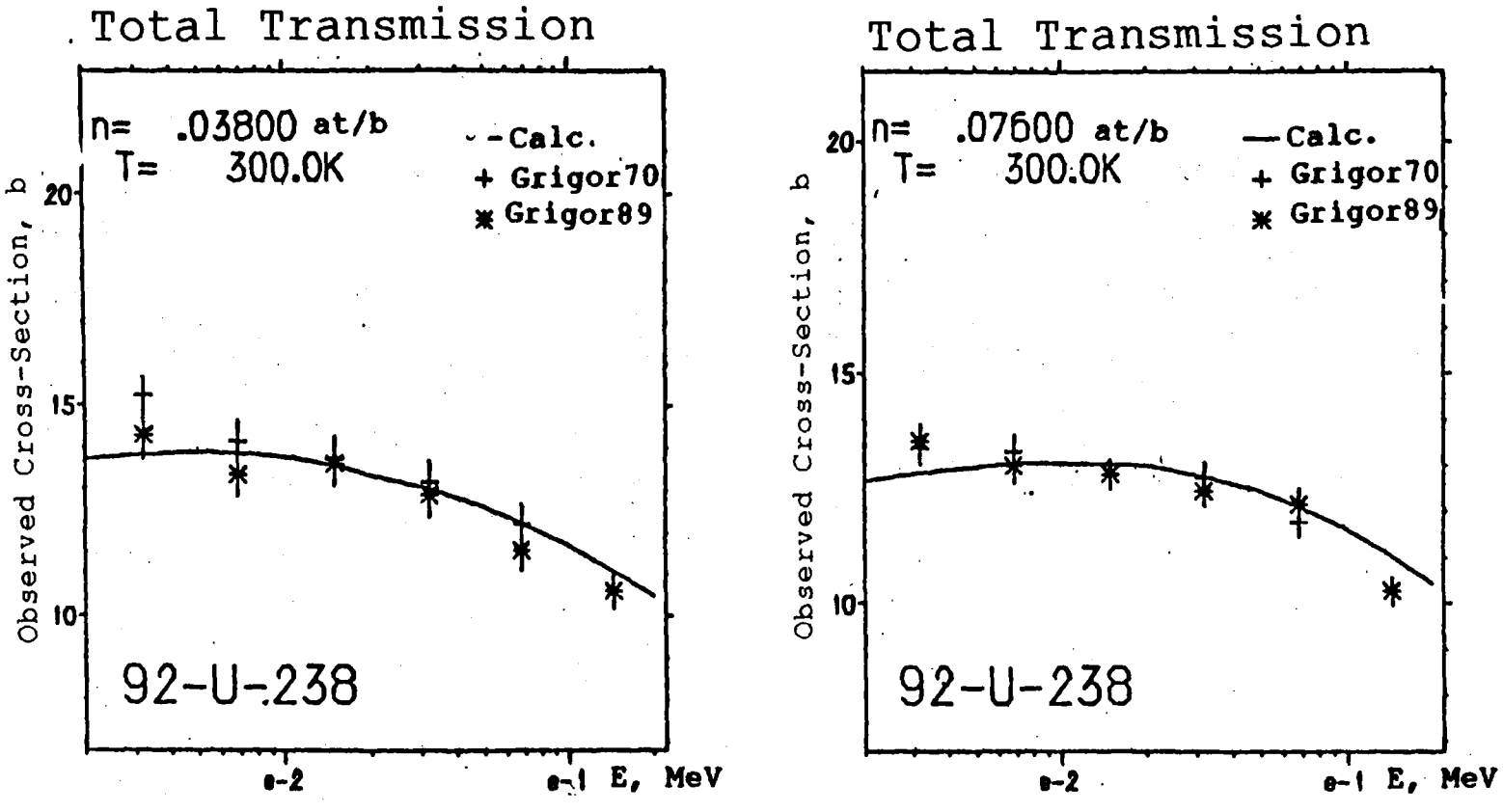

Fig. 3 Energy dependence of the observed cross-section for 8 and 16mm uranium-238 filter samples.

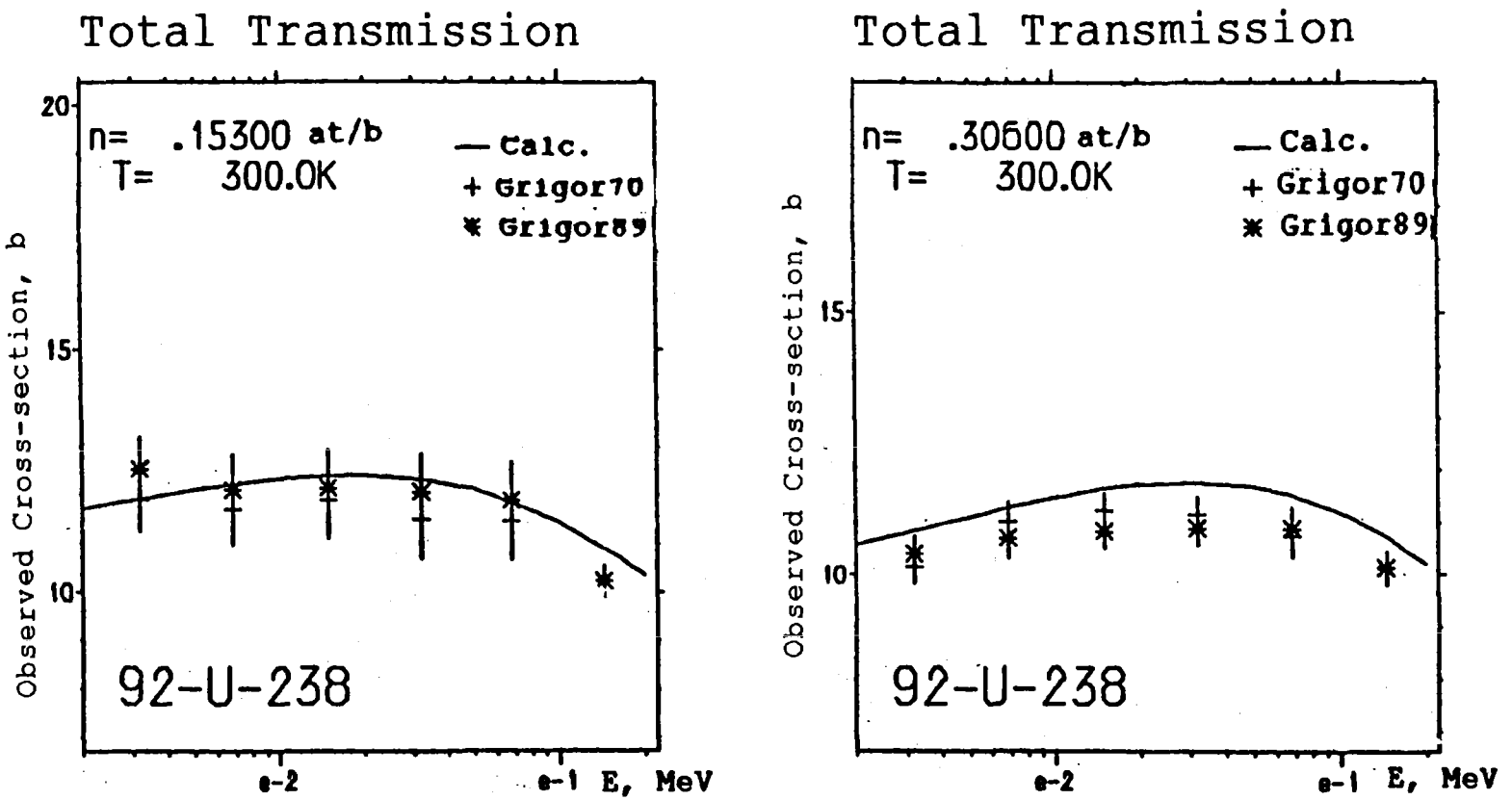

Fig. 4 Energy dependence of the observed cross-section for 32 and 64mm uranium-238 filter samples

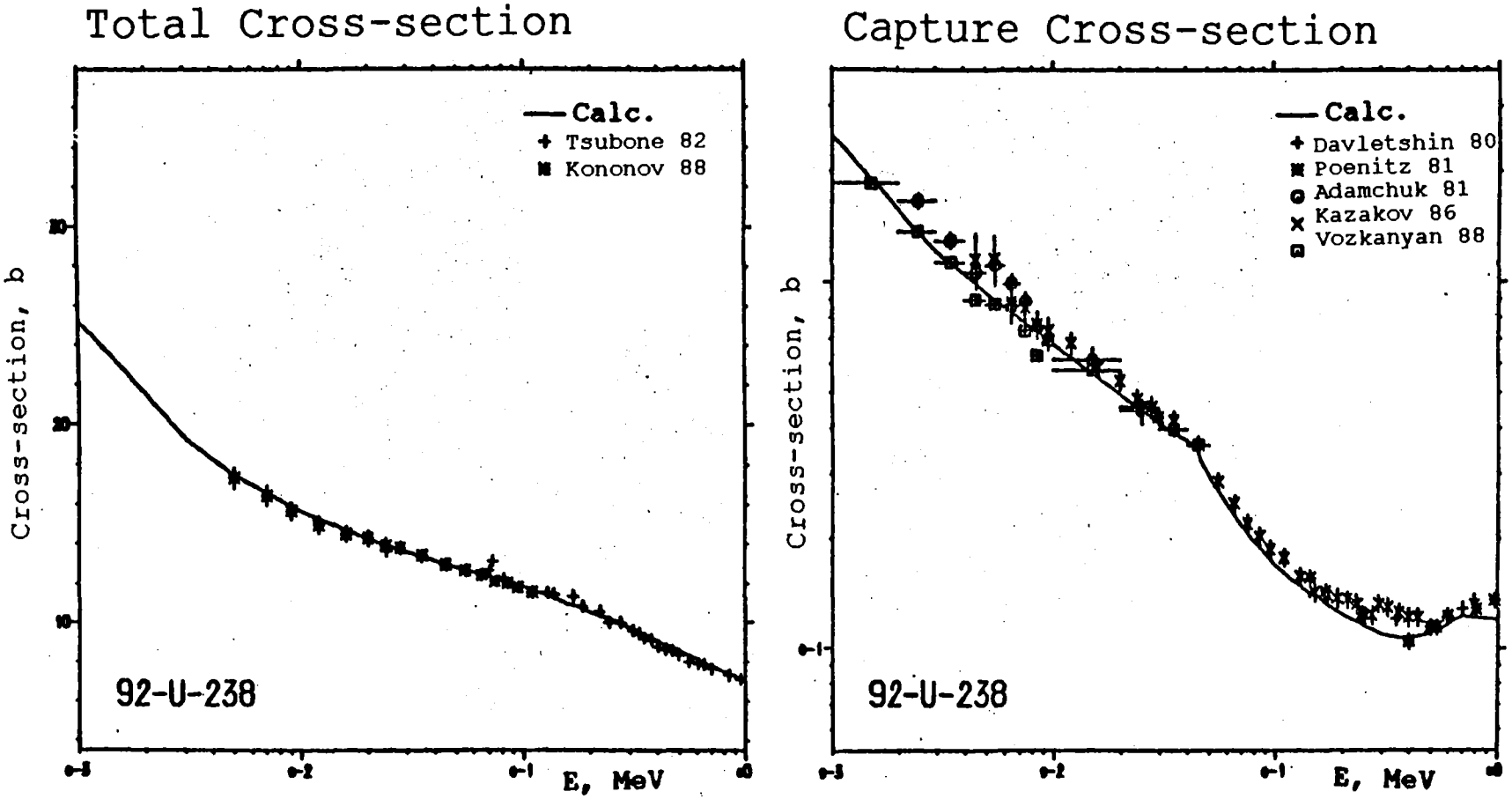

Fig. 5 Total and radiative capture uranium-238 cross-sections in the 1-1000 keV energy range

REFERENCES

[1] ABAGYAN, L.P., BAZAZYANTS, N.O., BONDARENKO, I.I., NIKOLAEV, M.N., Group Constants for Nuclear Reactor Calculations, Atomizdat, Moscow (1964) [in Russian].

[2] ABAGYAN, L.P., BAZAZYANTS, N.O., NIKOLAEV, M.N., TSIBULYA, A.M., Group Constants for Reactor and Protection Calculations, Ehnergoizdat, Moscow (1981) [in Russian].

[3] VAN'KOV, A.A., GRIGOR'EV, Yu.V., NIKOLAEV, M.N., et al., Proc. Conf. on Nuclear Data for Reactors, Helsinki 1970, Vol.1, IAEA, Vienna Vol.1 (1970) 559.

[4] BYOUN,T.Y., BLOCK, R., SEMLER, T., In: Proc. Nat. Top. Mect. on New Developments in Reactor Physics and Shielding, September 1972, New York, USAEC 115.

[5] GRIGOR'EV, Yu.V., BAKALOV, T., ILCHEV, G., Measurement of Resonance Self-Shielding Effects in the Scattering Cross-Section in the 1-100 keV Neutron Energy Region, Preprint FEhI-1216, Obninsk (1981) [in Russian].

[6] PEREZ, R.B., SAUSSURE, G. de, YANG, T., et al., Trans. Amer. Nucl. Soc. 44 (1983) 337.

[7] KAZAKOV, L.E., KONONOV, V.N., MATUROV, G.N., et al., Vopr. Atomnoj. Nauki i Tekhniki, Ser.: Yad. Konstanty 3 (1986) 37 [in Russian].

[8] FUZHITA, I., KOBOYASHI, R., KOMAMOTO, S., et al., Neutron Physics (Proc. 1st Int. Conf. on Neutron Physics, Vol. 2), Kiev-Moscow (1988) 195 [in Russian].

[9] BOKHOVKO, M.V., KONONOV, V.N., MANTUROV, G.N., et al., Vopr. Atomnoj. Nauki i Tekhniki, Ser.: Yad. Konstanty 3 (1988) 11 [in Russian].

[10] GEORGIEV, G.P., GRIGOR'EV, Yu.V., ERMAKOV, V.A., et al., Device for Measuring Neutron Cross-Sections and Radiation Multiplicity in the Interaction of Neutrons with Nuclei, Report of the OIYaI [Joint Nuclear Research Institute] R3-88-555, Dubna (1988) [in Russian].

[11] GRIGRO'EV, Yu.V., SIRAKOV, I.A., KHRYKINA, T.D., TISHIN, V.G., Measurement Module with the "FORD" Control Program for Investigating the Resonance Structure of Neutron Cross-Sections, Preprint FEhI-2060, Obninsk (1989) [in Russian].

[12] NIKOLAEV, M.N., KHOKHLOV, V.F., Nuclear Data Information Centre Bulletin 4 (1967) 420 [in Russian].

[13] FILIPPOV, V.V., Vopr. Atomnoj Nauki i Tekhniki, Ser.: Yad. Konstanty 4 (1985) 33 [in Russian].

[14] GRIGRO'EV, Yu.V., Measurement of Neutron Cross-Sections and Resonance Characteristics for ^{238}U on the IBR Spectrometer, Abstract of thesis for Candidate's degree, OIYaI, Dubna (1980) [in Russian].

[15] VAN'KOV, A.A., UKRAINTSEV, V.F., Vopr. Atomnoj. Nauki i Tekhniki, Ser.: Yad. Konstany 4 (1987) 58 [in Russian].

[16] MANTUROV, G.N., NIKOLAEV, M.N., Neutron Physics (Proc. First Int. Conf. on Neutron Physics, Vol. 1), Kiev-Moscow (1988) 440 [in Russian].

[17] ENDF-102, Data formats and procedures for the evaluated nuclear data file, ENDF/B-V, BNL-NCS-50496 (1983).

[18] SINITSA, V.V., Vopr. Atomnoj Nauki i Tekhniki, Ser.: Yad Konstanty 5 (59) (1984) 34 [in Russian].

[19] MANTUROV, G.N., LUNEV, V.P., GORBACHEVA, L.V., Neutron Physics (Proc. 6th All-Union Conf. on Neutron Physics, Vol. 2), Moscow (1983) 231 [in Russian].

[20] VAN'KOV, A.A., GOSTEVA, L.S., UKRAINTSEVA, V.F., Vopr. Atomnoj Nauki i Tekhniki, Ser.: Yad. Konstanty 3 (1983) 27 [in Russian].

Submitted for publication on 25 July 1991.

THERMAL NEUTRON FISSION CROSS-SECTIONS AND FISSION RESONANCE INTEGRAL OF ^{238}Pu

V.S. Zenkevich, Yu.A. Selitskij, V.B. Funshtejn and V.A. Yakovlev
I.V. Kurchatov Institute of Atomic Energy
Moscow

ABSTRACT

The fission cross-sections and the resonance integral values were measured on the F-1 reactor. The ^{238}Pu sample was irradiated in a reactor thermal column at a thermal neutron flux density of 1.6×10^7 $cm^{-2} \cdot s^{-1}$. The fission resonance integral was measured in a horizontal channel with a (1/E) resonance neutron flux density of 6×10^7 $cm^{-2} \cdot s^{-1}$. ^{239}Pu and ^{235}U were used as standards. The values obtained for ^{238}Pu are σ_f = 16.7 +0.8 barn, and I = 26.3 $\pm$ 1.5 barn.

At the present time ^{238}Pu is used as an energy source in medicine and space technology. To determine the rate of build-up of ^{238}Pu in reactor fuel, we need to know the ^{238}Pu fission cross-sections in the thermal and resonance neutron energy regions as well as the cross-sections of the (n,γ) and (n,2n) reactions in order to estimate burnup. The fission cross-sections of ^{238}Pu in the thermal spectrum (σ_f) and the resonance integral (I_f) have already been measured [1-5]. Data from these experiments are given in the table. As can be seen the measured σ_f and I_f values show significant spread and, in addition, the I_f values have a high experimental error.

Values of the fission cross-section in the thermal neutron spectrum and the fission resonance integral of ^{238}Pu

σ_f, barn	I_f, barn	Reference
18 ± 2	-	[1]
20	-	[2]
18.40 ± 0.9	-	[3]
17	-	[4]
17.1 ± 0.4	32 ± 5	[5]
16.5 ∓ 0.5*	24 ± 4	[6]

* Fission cross-sections σ°_f for E_n = 0.0253 eV.

In the present study ^{238}Pu was obtained from the alpha decay of ^{242}Cm, previously separated from plutonium. The target, prepared by spraying in a vacuum, contained 2.10 ± 0.1 μg of ^{238}Pu and 10.6 ± 0.5 ng ^{239}Pu. The amount of ^{239}Pu in the target was determined from the area under the 0.3 eV resonance; using this target, the energy dependence of the fission cross-section was measured with a spectrometer by determining the neutron slowing-down time in lead [7]. The ^{238}Pu target was irradiated in a thermal column in the F-1 reactor at the Kurchatov Institute of Atomic Energy. The neutron flux density was 1.6 x 10^7 $cm^{-2} \cdot s^{-1}$ with a cadmium to $^{235}U(n,f)$ ratio of 600. The measurement of the fission resonance integral was carried out in a horizontal channel of the F-1 reactor in a resonance neutron flux density (1/E) of 1.6 x 10^7 $cm^{-2} \cdot s^{-1}$ and cadmium to ^{55}Mn, ^{63}Cu and $^{235}U(n,f)$ ratios of 14, 14 and 30, respectively. The thickness of the cadmium shield was 1 mm. The standard targets used were a ^{239}Pu target with a mass of 38.3 ± 0.3 ng and a ^{235}U target with a mass of 260 ± 13 ng. The weight of the ^{235}U target was determined using the alpha particle backscattering method. Fission fragment were detected on mica detectors [8]. The standard values of σ_f and I_f for ^{235}U and ^{239}Pu were taken from the handbook [9]: the thermal neutron fission cross-sections measured in a Maxwellian spectrum was found to be $\sigma_f(^{239}Pu) = \sigma^{\circ}_f \times g_o = 780.8 \pm 1.8$ b, where σ°_f is the neutron fission cross-section for E_n = 0.0253 eV, g_o is the Westcott factor for T = 290°K; $I_f(^{235}U) = 280$ b.

The resulting values obtained for ^{238}Pu were σ_f = 16.7 ± 0.8 b and I_f = 26.3 ± 1.5 b (cut-off energy 0.5 eV). Comparison of the measured values with the data in the table shows that in the present study the error in $I_f(^{238}Pu)$ determination has been reduced considerably.

REFERENCES

[1] REED, G., MANNING, W.M. and BENTLEY, W.C., Report. ANL-4112 (1942).

[2] HANNA, G.C., HARVEY, B.G., MOSS, N. and TUNNICLIFF, P.R., Phys. Rev. 81 (1951) 893.

[3] HULET, E.K., HOFF, R.W., BOWMAN, H.R. and MICHEL, M.C., Phys. Rev. 35, p.147.

[4] BUTLER, J.R., LOUNGSBURY, M., MERRIT, J.S., Canad. J. Phys. 35 (1957) 147.

[5] EASTWOOD, T.A., BAERY,A.P., BIGHAM,C.B., et al., Proc. Geneva Conf. 1958, P/203, Vol.16, p.54.

[6] Neutron Cross-Sections, BNL-325, 3rd ed. Vol.1 (1973); part A (1981).

[7] GERASIMOV, V.F., DANICHEV, V.V., DEMENT'EV, V.N., et al., "Measurement of the fission cross-section of transuranic elements on a spectrometer with respect to the slowing-down time in lead" Voprosy atomnoj nauki i tekhniki. Ser. Obshchaya i yadernaya fizika. 3, 36 (1986) 43.

[8] RUMYANTSEV, O.V., SELITSKIJ, Yu.A. and FUNSHTEJN, V.B., "Fission fragment recording using mica by subjecting the detector to intensive charged particle irradiation", Pribory i Tekhnika Ehksperimenta 1 (1986) 51.

[9] Handbook on Nuclear Activation Data, Technical Reports Series 1987, No. 273, Vienna, IAEA.

Submitted for publication 6 August 1990.

ABSOLUTE MEASUREMENTS OF THE ^{237}Np AND ^{233}U FISSION CROSS-SECTIONS AT 1.9 MeV NEUTRON ENERGY USING THE TIME-CORRELATED ASSOCIATED PARTICLE METHOD AND A MAGNETIC ANALYZER

V.A. Kalinin, S.S. Kovalenko, V.N. Kyz'min,
Yu.A. Nemilov, L.M. Solin, V.I. Shpakov

ABSTRACT

Absolute measurements of the ^{233}U and ^{237}Np fission cross-sections have been performed at a 1.9MeV neutron energy by means of the time correlated associated particle method. The $D(d,n)^3He$ reaction was used as the neutron source. The associated particles were separated from the background by using a magnetic separator. Application of magnetic analysis permitted the use of the TCAP technique to make measurements at a neutron energy of about 2 MeV. A silicon surface barrier detector was used to detect the associated particles. The fission fragments were registered by means of a parallel plate ionisation chamber. The following results were obtained: $\sigma_f(233U) = 1.93\pm0.07$ b, $\sigma_f(237Np) = 1.73\pm0.05$ b.

The time-correlated associated particle method (TCAP) is now widely acknowledged as the most accurate and reliable method for absolute measurements of fission cross-sections. The underlying principle of the method is that the neutron flux passing through a fissile isotope target is based on the number of recorded associated particles, namely ^3He or ^4He ions,or helions, which are generated in the neutron source reaction $D(d,n)^3He$ or $T(d,n)^4He$. The deuterium or tritium is contained in thin transit targets. Assuming that all neutrons in a given solid angle (neutron cone), (which according to the reaction kinematics corresponds to the solid angle of helion counts), strike the target of fissile material and the heterogeneity of the target is relatively low, the fission cross section can be described by the

simple formula:

$$\sigma_f = N_c/nN_{He} \qquad [1]$$

where N_c is the number of coincidence counts, n is the number of target nuclei per cm^2 and N_{He} is the number of counted associated particles.

The TCAP method has the following advantages:

- There is no need to measure the total neutron flux, or the full associated particle integral;
- Fission events caused by background neutrons are virtually excluded;
- Anisotropic effects related to the anisotropy of neutron emission from the target are excluded;
- The calculation of geometrical factors is reduced to a minimum.

The TCAP method is thus the only one of the various absolute methods of neutron cross-section measurement which does not require a knowledge of the neutron flux monitor's efficiency. This reduces the probability of systematic errors. In view of the above advantages, the TCAP method measurements can be recommended [1] as the most likely to improve the accuracy of fission cross-section data in the future. Such data include fission cross-sections for the ^{237}Np and ^{233}U isotopes, which are very important in the thorium fuel cycle. Furthermore, ^{237}Np (together with ^{238}U) is considered as a possible threshold standard. Virtually all data on fast neutron fission cross-sections for these isotopes have been obtained in measurements relative to the ^{235}U fission cross-section. Absolute measurements were made by the TCAP method for only a few neutron energy values, and for these isotopes are virtually non-existent in the 1.5-2.5 MeV energy range. The aim of this paper is to fill these gaps.

The TCAP method for the neutron energy range 1.5-2.5 MeV

In practice it is difficult to achieve high reliability in experimental results using the TCAP method mainly because the associated particles are necessarily recorded against a high background level of charged particles. The background source consists of elastically scattered deuterons and products of secondary reactions between beam deuterons and target nuclei. There are at present two groups of fission cross-sections measurements using the TCAP method differing only in the way in which the associated particles are separated from the charged particle background. The choice of one or the other method, for a particular neutron source reaction, determines the permissible neutron energy or the neutron energy range. These groups are:

- Measurements in the neutron energy range of approximately 2.6 MeV [2, 3] for which the neutron source is the $D(d,n)^3He$ reaction and in the 14-15 MeV range [2, 4-7] for which the neutron source is the $T(d,n)^4He$ reaction. Low energy deuteron beams (on the order of a few hundred keV) were used and the scattered particles were completely stopped by a foil placed in front of the detector;
- The measurements for neutron energies of 4.5 and 8.5 MeV [8, 9], were carried out using a (ΔE-E) telescope in the associated particle channel.

This paper describes the application of the TCAP method to the measurement of the fission cross-section in the neutron range of 1.5-2.5 MeV, in the vicinity of the neutron fission spectrum maximum. The reaction $D(d,n)^3He$ was used as the neutron source. It follows from the kinematics of this reaction that the neutrons entering the lower hemisphere at large angles (no less than 130°) (see fig. 1),will have an energy in the range indicated. Meanwhile, the beam deuterons will have an energy of approximately 3 MeV. It is clear from fig. 1 that under the given conditions the neutron energy is only slightly dependent on the deuteron energy. This leads to a negligible neutron energy

spread caused by the slowing down of the deuterons during their transit through a target of deuterated polyethylene.

It follows that the dependence of the relative neutron energy spread on their emission angle (Fig. 2), that by choosing large neutron emission angles causes a reduction in the spread of their energies within the boundaries of the neutron solid angle. Thus, the given experimental configuration pre-determines a low neutron energy spread, which is particularly important for measurements in the range where the cross-section changes rapidly with neutron energy. However, the choice of large neutron emission angles leads to the recording of helions at low (7o-20o) relative to angles of the incident beam. At such angles the Coulomb scattering differential cross-section for beam deuterons on carbon nuclei contained in the target exceeds the D(d,n^{3}He) reaction by a factor of more than 10^3. As a result the flux of charged particles striking the associated particle detector is so intense, that it is difficult in practice to use the (ΔE-E) method to isolate helions from the background. Nor is it possible to use foils to absorb the scattered deuterons as their ranges are greater than the ^{3}He ranges.

Under these conditions the problem of reducing the background in the associated particle channel (which also means the correct determination of the magnitude of $N_{He)}$) was resolved by separating the ^{3}He trajectories from the homogenous charged particle background field, using a sector magnet. A diagram of the particle trajectories and the boundaries of the homogeneous magnetic field in the plane of the pole gaps of the magnet is shown in Fig.3. The magnetic field prevents the D(d,p)T reaction products from striking the detector, as their trajectory radii of curvature are approximately twice as large as those of the ^{3}He particles. The radii of curvature of the scattered deuterons in the magnetic field are 1.5 times greater than those of the helions. However, it was impossible to eliminate the deuteron background entirely, as a low-energy tail is created during their transit through the target. This is caused by the effects of

angular and energy straggling in their spectrum, and particles of this tail strike the associated particle detector in the uniform magnetic field. Nevertheless, the use of the magnetic field made it possible to reduce the flux intensity of the scattered deuterons striking the detector by more than a factor of 10^2. The use of deuterated polyethylene targets leads to the generation of additional groups of charged particles, i.e. protons which are either knocked out of the target by the beam neutrons, or produced by the ^{12}C d,p)^{13}C reaction. The protons knocked out of the target (the target contains approxmately 3% hydrogen), and the protons from the above reaction lead to the production of first excited states of the ^{13}C nuclei which have trajectories similar to those of the associated particles. Owing to the finite dimension of the detector they are recorded together with the ^3He and in turn form an additional background in the associated particle window. The proton background can be suppressed entirely if the particles are recorded by a silicon surface-barrier detector with a depleted zone depth of less than the range of a proton of a given energy in the silicon, but greater than the ^3He range.

The use of a magnetic analyzer in the associated particle channel permits on the one hand a maximum reduction of the charged particle background, and on the other hand makes it difficult to achieve a high enough ^3He counting rate required for real-time measurements. The problem is that losses in the associated particle counting rate may be caused as a result of a large scale image of the ^3He source at the exit from the magnetic field. Two factors are responsible for the increase in the image size: firstly, the particles travel a considerable distance from the source to the detector - 60-70 cm (within a finite recording solid angle, which is determined by the slit collimator at the entrance to the magnetic field); secondly, due to the slowing down of the ^3He particles, formed by the reaction at a different target depth (the thickness of the deuterated polyethylene film is approximately 1 mg/cm^2), there is additional spatial diversion of the ^3He particles trajectories in the plane of the reaction

which occurs during their transit through the magnetic field.

The influence of the first factor is partly compensated by the selected ratio of the neutron and ^{3}He emission angles. The reaction kinematics in this case are such that there is a three-fold decrease in the angular divergence of the outgoing ^{3}He particles in relation to the angle of the neutron cone. This makes it possible to reduce the horizontal dimension of the associated particle detector. In the vertical plane a reduction in the charged particle source image at the detector position is caused by the particles experiencing the influence of a local field boundary as they approach the homogenous magnetic field zone. The diminishing magnetic field at the pole gap boundary has the property of vertical focusing. Using the relationship $f = \rho/\mathrm{tg}\alpha$ as a basis (where f is the distance from the source to the field boundary (focus); ρ is the radius of curvature of the particle trajectory in the magnetic field; α is the angle between the particle trajectory and the normal to the field boundary), the appropriate instrument parameters were chosen so that the vertical dimension of the source image at the exit from the field should not exceed the dimension of the pole gap. The effectiveness of the vertical focusing is substantiated by the results of neutron solid angle profile measurements in the reaction plane and in the vertical plane, which were determined by coincidence counting of helions and neutrons, the latter being recorded by a scintillation counter with an angular dimension of 2°. The neutron solid angle profiles are shown in Fig. 4. It is clear from this figure that the apex angle of the neutron solid angle in the vertical plane is not smaller than in the horizontal plane and this is only possible with vertical focusing of the outgoing charged particles. As a result, a detector having dimensions 25 x 45 mm^2 was sufficient to avoid virtually any loss in the associated particle count. An additional measure to increase the neutron yield was rotation of the neutron source which is essential to ensure a maximum period of operation.

The resulting average velocity of the associated particle

count was $(1.5\text{-}2.0)10^3$ s^{-1} with a background level under the helion peak of no more than 0.1%. The amplitude spectrum in the associated particle channel is shown in Fig. 5.

Fission fragments were recorded by the traditional method of a methane-filled multi-layer ionization chamber at atmospheric pressure. The targets were prepared by high-frequency sputtering on an eccentric rotating platform. The surface density of the applied material for each target was determined by α-counting in a small-scale geometry . The uniformity of the layer was determined by measuring the α-activity from various parts of the targets using slit filters of appropriate dimension. The isotope component of the ^{233}U targets is shown in Table 1. The impurity content, determined from the α-activity of the ^{237}Np target is negligibly low. Table 2 shows the target surface densities and their radial heterogeneity characteristics.

The main characteristics of the experiment are as follows:

Neutron energy, MeV:	
^{233}U	1.94 ± 0.03
^{237}Np	1.90 ± 0.03
Deuteron energy	2.7 MeV
Target thickness (neutron source)	2.1 ± 0.1 mg/cm²
Emission angle for ^3He	14.0° ± 0.5°
Plane recording angle for ^3He	4°
Speed of ^3He count	$(1.5\text{-}2.0) \times 10^3$ s^{-1}
Induction of magnetic field	5×10^3 Gs
Associated particle detector	silicon, surface-barrier 25 x 45 mm², zone depth 45μ
Neutron emission angle:	
^{233}U	139° ± 1°
^{237}Np	141° ± 1°
Neutron solid angle width at the 0.1% level	19°
Angular dimension of farthest target:	
^{233}U	21°
^{237}Np	17.5°

Block diagram of the experiment

The above solution to the problem of separating associated particles from the background substantially improves the reliability of the final result. However there are other sources of error, including those relating to adjustments in the various components of equation(1). The accuracy of the corrections depends mainly on the level of completeness of the experimental data. This requirement can be met, and the various parameters of the measurement process monitored, by a computer-based system for the storage and control of the experimental data. Such a system was implemented using the KAMAK module standard and the "Ehlektronika H MCOIIOO.I" micro computer, on-line with a CM-4 mini computer. The following data were recorded during the experiment:

- The number of associated particles, the number of coincidences and the number of spurious coincidences;
- The spectrum of fission fragments with discrimination of noise from the amplifying channel and target α-activity, the complete fragment spectrum and the fragment spectrum in coincidence with the associated particles (this group of spectra makes it possible to have a relatively accurate assessment of losses in the recording of coincidences connected with discrimination in the fragment channel, as well as controlling during the measurement the amplification coefficient in that channel, which may decrease with the ageing of the gasin the ionization chamber);
- The time spectrum of spurious coincidences and the spectrum in the coincidence window (these spectra are essential for adjusting the background of spurious coincidences and for monitoring time delays between channels, which ensure recording of coincidences in the "window", defined by fast logic circuitry).

The blocked diagram of the recording system is shown in Fig. 6. The electrical pulses from the associated particle detector and the ionization chamber are amplified and then each one if channeled to the appropriate monitoring threshold shaping unit (MTS) and pulse

"stretcher". The MTS processes the time-tagged pulses required for operation of the time-amplitude converter (TAC) and the rapid coincidence circuitry. The time-delayed fragment-associated particle spectra, converted to amplitude spectra are recorded with the aid of corresponding analogue-to-digital converters (ADC). The pulse "stretcher" is used to extract spectral information from the source signals. With its help the fast current signals are transformed into a voltage surge required for the operation of the ADC. A microcomputer compiles, sorts and monitors the data and then an ordered set of data are recorded on magnetic discs by the CM-4 minicomputer.

Measurement results

The final fission cross-section value was arrived at by taking the above corrections into account. Losses in the fission event count were determined by the traditional method - by introducing corrections for discrimination in the fragment channel, which was determined by extrapolation of the fragment spectrum to zero amplitude, as well as corrections for fragment absorption in the layer of the fissile material. The latter was calculated taking fission anisotropy and neutron pulse transmission spread into account using the formula proposed in Ref. [11]. The average fragment range was 5.9 mg/cm^2.

The adjustment for spurious coincidences was determined by analyzing the time spectrum of fission fragment associated particles coincidences. The adjustment for neutron flux perturbation caused by scattering on components of the experimental instrumentation and target support structure was solved by considering it an inverse radiation transport problem. The transport equation was solved by the Monte Carlo method [12]. In addition, corrections were made for contaminants of fissile isotopes in the target material. Their cross-sections were taken from the ENDF/B-V library. The values for the corrections and accuracy of the results are shown in Table 3. Table 4 compares cross-sections presented in this paper with data from ENDF/B evaluations.

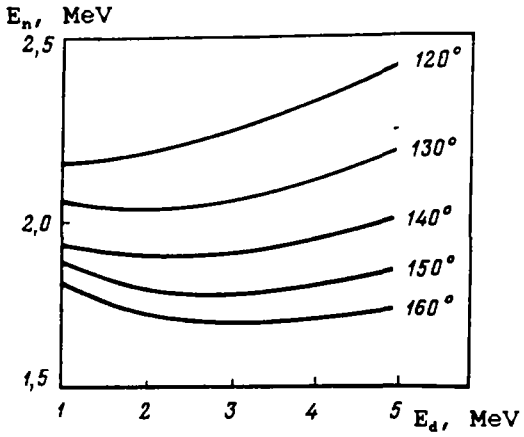

Fig. 1. Neutron energy dependence in the D(d,n)^{3}He reaction on the deuteron energy for various neutron emission angle (E_n and E_d are the neutron and deuteron energies respectively)

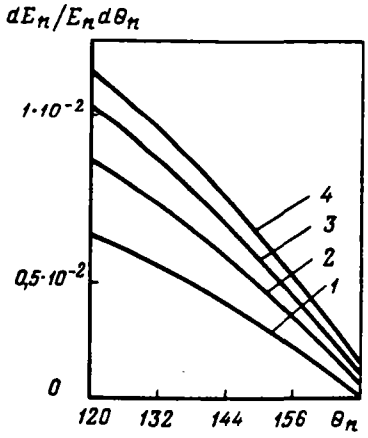

Fig. 2. Dependence of the relative neutron energy spread in the D(d,n)^{3}He on the emission angle θ_n in the reaction plane. The deuteron energies are given in MeV.

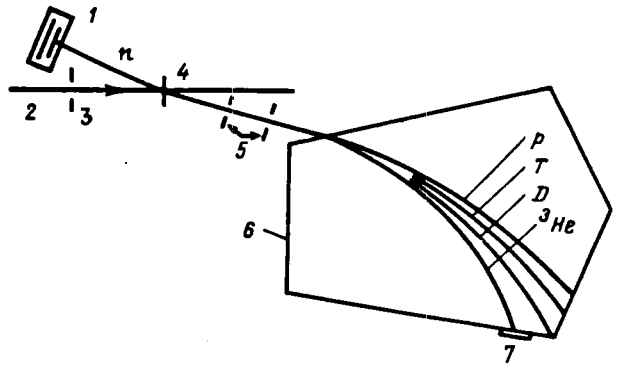

Fig. 3. Diagram of the TCAP method using magnetic analysis in the associated partical recording channel, showing the trajectories of protons (p) and tritons (T) from the D(d,p)T reaction and scattered deuterons and associated particles (^{3}He):1 - ionization chamber; 2 - deuteron beam from electrostatic accelerator; 3 - deuteron beam collimator; 4 - deuterated polyethylene target; 5 - slit collimators to determine the associated particle solid recording angle;6 - boundary of homogeneous magnetic field; 7 - associated particle detector.

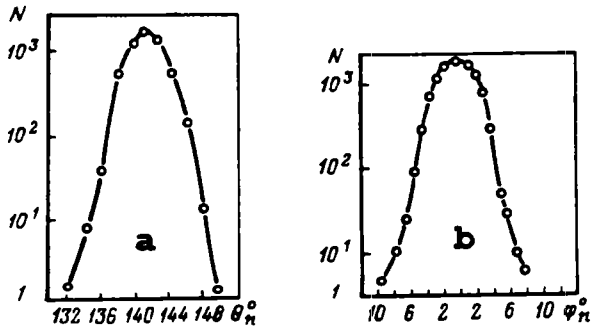

Fig. 4. The neutron cone profile in the reaction plane (a), and in the vertical plane (b); θ_n is the neutron emission angle in the reaction plane, φ_n is the azimuthal neutron emission angle, and N is is the number of associated particle-neutron coincidences.

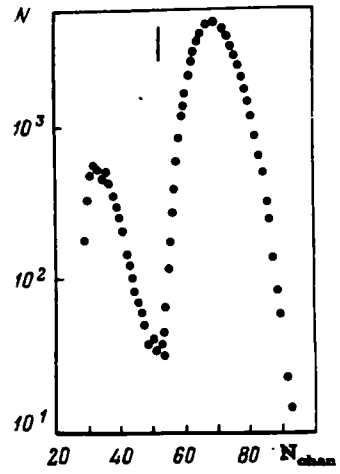

Fig. 5. Amplitude spectrum in the associated particle recording channel. The vertical line indicates the discrimination threshold of these particles; N is the number of counts and N_{chan} is the channel number.

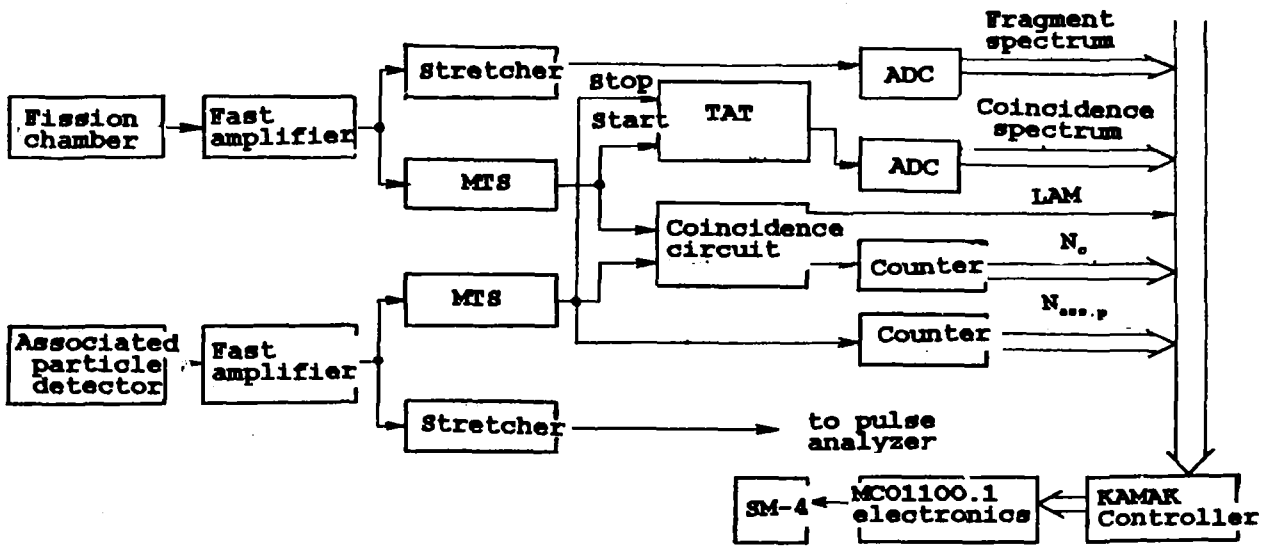

Fig. 6. Block diagram of the electronic system for the processing of experimental data

Table 1

Isotopic composition of fissile material in ^{233}U targets (mass spectrometer data)

Isotope	Isotope content, %	Half-life, y [10]
^{233}U	82.899±0.100	(1.592±0.002) $\cdot 10^5$
^{234}U	0.332±0.014	(2.454±0.006) $\cdot 10^5$
^{235}U	0.141±0.010	(7.037±0.011) $\cdot 10^8$
^{238}U	16.628±0.038	(4.468±0.055) $\cdot 10^9$
^{232}U	<0.003	69.8±1.0

Table 2

Surface densities of fission targets and characteristics of their radial non-homogeneity, relative units

Isotope	Surface density, g/cm^2	Distance from center, mm			
		0	3	6	9
^{233}U	0.214	1.000	1.004	1.004	0.990
	0.255	1.000	0.999	1.002	1.002
^{237}Np	0.245	1.000	0.998	1.014	0.989
	0.250	1.000	1.001	1.001	1.006
	0.195	1.000	1.014	1.004	1.007

Table 3

Corrections and errors in experimental results, %

Source of error	^{233}U		^{237}Np	
	Correction	Error	Correction	Error
1	-	3	-	1.9
2	13.3	1.1	4.7	0.7
3	1.8	0.6	4.5	0.7
4	1	0.3	0.95	0.30
5	-	2	-	2
6	4.5	0.2	-	-
7	0.2	0.1	0.2	0.1
8	3.8		2.9	

1 - Coincidence statistics
2 - Random coincidence background
3 - Extrapolation of fragment spectrum to zero
4 - Absorption of fragments in target material layer
5 - Weighing of targets
6 - Admixture of ^{238}U in ^{233}U targets
7 - Scattering of neutrons on hardware components
8 - Total error

Table 4

Comparison of cross-section data

Nuclide	Cross-section, barns		
	This paper	ENDF/B-4	ENDF/B-5
^{233}U	1.93±0.07	1.89	-
^{237}Np	1.73±0.05	-	1.66

REFERENCES

[1] INTERNATIONAL ATOMIC ENERGY AGENCY, ^{235}U Fast Neutron Fission Cross-sections (Proc. Cons. Mtg., Smolenice, CSSR, 1983), Report INDC(NDS)-146, Vienna (1983) 13.

[2] ARLT, R., GRIMM, W., JOSH, M., et al., (in Proc. Intern. Conf. on Nuclear Cross-sections for Technology, Knoxville, USA, 1979), NBS Special Publication No.594, Washington (1980) 990.

[3] ALKHAZOV, I.D., VITENKE, V.A., DUSHIN, V.N., et al., (in Proc. 10th Intern. Symp. on the Interaction of Fast Neutrons with Nuclei, Gaussig, GDR, 1981), Report ZFK-459, Dresden (1981) 44.

[4] WASSON, O.A., MEIER, M.M., DUVALL, K.C., Nucl. Sci. Eng. 80 (1982) 882.

[5] LI JINGWEN, LI ANLI, RONG CHAOFAN, et al., (in Proc. Intern. Conf. on Nuclear Data for Science and Technology, Antwerp, 1982), Holland (1983) 55.

[6] ADAMOV, V.M., ALKHAZEV, I.D., GUSEV, S.E., et al., ibid. ref.[2] p.995.

[7] CANCE, M., GRENIER, C., Nucl. Sci. Eng. 68 (1978) 197.

[8] ARLT, R., HERBACH, C.M., JOSCH, M., et al., (in Proc. Adv. Group Mtg. on Nuclear Standards and Reference Data, Geel, Belgium, 1984), Report IAEA-TECDOC-335, Vienna (1985) 174.

[9] ARLT, R., Josch, M., MUSIOL, G., et al., ibid. ref [3] p.35.

[10] INTERNATIONAL ATOMIC ENERGY AGENCY, Proposed Recommended List of Transactinium Isotope Decay Data, Part I; Half-Lives, Report INDC(NDS)-149, Vienna (1983) 8.

[11] ARLT, R., et al., Techn. Univ. of Dresden, Preprint 05-5-79, Dresden (1979).

[12] DUSHIN, V.N., (in Proc. 8th Intern. Symp. on the Interaction of Fast Neutrons with Nuclei, Gaussig, GDR, 1978), Report ZFK-382, Dresden (1978) 153.

Submitted for publication 27 January 1987